IUBAT Review—A Multidisciplinary Academic Journal, 9(1): 49-67
https://doi.org/10.3329/iubatr.v9i1.91392

Numerical Investigation of Neon Soft X-ray and Ion Beam Characteristics in BARC Plasma Focus Device

Mohaiminul Islam Nayeem[1]*, Md Mahbubur Rahman[1]

[1]*Department of Physics, IUBAT- International University of Business Agriculture and Technology, Dhaka, Bangladesh*

Key Words:

BARC PF device; Electrode Optimization; Lee code; Neon Gas; Soft X-rays

Abstract

A numerical investigation on the Bhabha Atomic Research Centre (BARC) plasma focus (PF) machine has been performed with the Lee model code (RADPF5. 16FIB) for characterizations of SXR emission and the ion beam using neon (Ne) as a working gas. The simulations were run using the device set at 11.5 kJ capacitor bank energy, and the results analyzed at various operating pressures and electrode geometries. For SXR emission, the calculated pinch plasma temperature of SXR yield from neon was in the range 2.3×10^6 - 5×10^6 K (200–500 eV), which is the region of full ionization of neon. The peak effective SXR power of 114.9 J at 1.75 Torr, which is ~1 % of the bank input energy. By optimizing the electrode geometry, the overall energy yield was increased to 137 J/shot with a = 3 cm, b = 6.8 cm, P_0 = 1.75 Torr, with which it was possible to reach 1.2% efficiency. Furthermore, for the ion beam characteristics, the ion beam fluence, flux, and focused ion beam (FIB) energy demonstrated distinct pressure-dependent behavior and achieved best performance at 1.75–2 Torr. These results demonstrate that the BARC PF can be a source of high-intensity pulsed SXR and high fluence ion beams, which is a compact, low-cost, and efficient radiation source for a variety of plasma diagnostic, material processing, and fusion relevant studies.

1. Introduction

The dense plasma focus (DPF) machines are intense pulsed plasma devices, which have been receiving a lot of attention since their first operation in the 1960s for their capability of generating energetic radiation and charged particle beams (Mather, 1971). The interplay between the current density and its associated magnetic field leads to the collapse of the short-lived plasma, known as the plasma pinching phenomenon in a PF device, belonging to the Z class pinches that generates super-dense (~10^{16}-10^{19} cm^{-3}), super-hot (~1 keV) plasma for a very short time (~100s ns) due to self-generated electromagnetic compression known as pinch (Mather, 1971). During this pinch, high-energy ion beam (~MeV) (Boggasch *et al.*, 1991; Fortov *et al.*, 1998) and electron beam (~1 MeV), soft X-rays (~100s eV) and hard X-rays (100s keV) (Pereira & Davis, 1988), pulsed fusion neutron (~14.5 MeV) (Velikovich *et al.*, 2007) are emitted. Among the different emissions, soft X-rays

*Corresponding author's E-mail address: nayeem.phy@iubat.edu
Article received: November 2025 Revised and accepted: April 2026 Published: June 2026

(SXR) play an important role due to their applications in X-ray lithography (using 0.9–1.5 keV photons) (Kato *et al.*, 1988; Lee *et al.*, 1998; Petr *et al.*, 2004; Wong *et al.*, 2004), contact microscopy (using 0.25–2.5 keV radiations) (Castillo-Mejía *et al.*, 2001; Rawat *et al.*, 2004), X-ray radiography (Beg et al., 2000; Hussain et al., 2005), and micromachining (using 4 keV photos) (Gribkov *et al.*, 2002). SXR emitting efficacy from a PF is a function of various factors, such as the type of filling gas, discharge energy, electrode geometry and the operational pressure. Neon is one of the best gases for SXR generation owing to its emission properties in the electron temperature range of 2.3×10^6 to 5×10^6 K (~200–500 eV), where the plasma is fully ionized (Akel *et al.*, 2012). Its identification and characterization and the maintenance of a plasma temperature within this window, are the key to the optimum radiation of the neon line. In addition to SXR investigations, ion beams that are delivered during the pinch phase are also of much interest for surface modification, ion implantation, and ion-assisted coating technologies, semiconductor doping etc. (Hayashi *et al., 1999;* Rosiński *et al., 2005;* Sadowski *et al., 2000;* Shi *et al., 2001;* Tomida *et al.*, 2005; Tong *et al.*, 1995; Wen *et al.*, 1986; Yatsui *et al.*, 1997). The ion fluence, flux, and beam energy show a strong pressure dependence that is controlled by the interaction between the plasma density, the confinement time, and the energy coupling from the capacitor bank. Thus, the demonstration of the simultaneous optimization of SXR emission and ion beam properties is important for developing the multi-functionalities of PF systems.

The PF dynamics are highly transient and complex, making experimental studies alone insufficient for a complete understanding. Numerical modeling, particularly with the Lee model code, has become essential as it integrates dynamic, electrodynamic, thermodynamic, and radiation processes into a self-consistent framework. Extensively benchmarked across devices from sub-kilojoule to megajoule scales, the code can reliably compute current waveforms, plasma trajectories, SXR yield, and ion beam parameters, making it a powerful tool for performance optimization (Soto *et al.*, 2008; Verma *et al.*, 2008; Wahbe *et al.*, 2023). In this work, the Lee model code (RADPF5.16FIB) (*Plasma Focus (Radiative) Computation Model*) is applied to the BARC PF device (11.5 kJ). The study investigates (i) optimization of neon SXR yield within the effective pinch plasma temperature range of 2.3×10^6 to 5×10^6 K, and (ii) ion beam properties—fluence, flux, and energy—under varying pressures. Electrode geometry is also explored for further optimization. The results define the efficient operating regime of the BARC PF and demonstrate its promise as a compact pulsed source of SXR and energetic ion beams.

2. Numerical Experiment

2.1 Soft X-ray and Ion Calculation in the Lee Code

The fundamental modeling of the Lee code, encompassing with axial and radial phases outlined in 1984 (McNamara, 1984), was effectively applied in various numerical studies (Lee, 1991; Lee *et al.*, 1988; Lee & Serban, 1996; Saw, 1990; Tou *et al.*, 1989). The incorporation of radiation-coupled dynamics within a 5-phase code has proven effective for conducting numerical experiments focused on radiation cooling (Ali, 1990). The five phases are designated as follows: (i) axial phase, (ii) radial inward shock phase, (iii) radial reflected shock (RS) phase, (iv) slow compression (quiescent) or pinch phase, and (v) expanded column phase (Saw *et al.*, 2009). The code has seen widespread implementation as an additional feature in several devices, including miniature pinch PF discharges operating at energies as low as 0.1 J, which enables comprehensive simulation capabilities (Pavez & Soto, 2010). The specifications, theoretical framework, code implementation, and a comprehensive array of outcomes from the "Universal Plasma Focus Laboratory Facility" are readily accessible for download at the specified location (*Plasma Focus (Radiative) Computation Model*). In this work, the numerical studies were employed in the latest version of the RADPF5.16FIB code (*The Universal Plasma Focus Machine*). In the Lee code, the calculation of line radiation Q_L is executed as follows:

$$\frac{dQ_L}{dt} = -4.6 \times 10^{-31}\frac{n_i^2 Z_{eff} Z_n^4 (\pi r_p^2) z_{max}}{T}$$

Where, Q_L is the hydrogen line radiation, Z_n is the atomic number, Z_{eff} is the effective number, n_i is the ion density, r_p the pinch radius, z_{max} is the pinch column length, and T is the average temperature of the pinch plasma.

Using the radiative Lee model code for the plasma focus, Lee and Saw (2013) calculated the characteristics of the ion beam and derived the flux equation for the ion beam. The exit beam is most accurately described by ion fluence, which is defined as the number of ions per unit cross-section, as the beam departs from the focus pinch with minimal divergence. The subsequent equations are employed following Lee and Saw (Lee & Saw, 2013)-

Flux (ions $m^{-2}s^{-1}$) = $J_b = 2.75 \times 10^{15} (f_e/[MZ_{eff}]^{1/2}) \times \{(\ln[b/r_p])/(r_p^2)\} (I_{pinch}^2)/U^{1/2}$
Fluence (ions m^{-2}) = $2.75 \times 10^{15}\, \tau\, (f_e/[MZ_{eff}]^{1/2}) \times \{(\ln[b/r_p])/(r_p^2)\} (I_{pinch}^2)/U^{1/2}$

The ion fluence (ions m^{-2}) is computed by multiplying the flux by pinch duration τ. Here, M is the mass number of the ion, b is the cathode radius, and $f_e = 0.14$ (the fraction of energy converted from pinch inductive energy into beam kinetic energy) is equivalent to the ion beam energy of 3%–6% E_0 (Akel *et al.*, 2014). The diode voltage U is $U = 3V_{max}$, taken from data fitting in extensive earlier numerical experiments (Akel *et al.*, 2014; Lee & Saw, 2013; *Plasma Focus (Radiative) Computation Model*), where V_{max} is the maximum induced voltage of the pre-pinch radial phase. The value of the ion flux is determined in each situation for a specific machine using a specific gas by computing the values of Z_{eff}, r_p, pinch duration (τ), pinch current (I_{pinch}), and U, using the Lee Model code configured with the specific machine's and gas's parameters. Once the flux is determined, the following quantities are also computed: power density flow (W m^{-2}), current density (A m^{-2}), current (A), ions per sec (ions s^{-1}), fluence (ions m^{-2}), number of ions in beam (ions), energy in beam (J), damage factor (W m^{-2} $s^{0.5}$), energy of FPS (J) (Akel *et al.*, 2014). The plasma diode impedance (Ω) and the constricting pinch magnetic field (kG) are also computed (Akel *et al.*, 2014).

2.2 Lee Code Configuration

Primarily, the measured discharge current derivative and the following device parameters of the BARC PF device are picked out from the published paper (Singh *et al.*, 2017):

Bank Parameters: Static inductance, L_0 = 77 nH, the capacitor bank's capacitance, C_o = 40 µF, Circuit stray resistance, r_o = 4 mΩ.

Tube parameters: Radius of the cathode, b = 6.1 cm, Radius of the anode, a = 3 cm, Length of the anode, z_o = 7.7 cm.

Model parameters: $f_m = 0.22$, $f_c = 0.7$, $f_{mr} = 0.22$, $f_{cr} = 0.72$.

Operating parameters: Operating voltage, V_o = 24 kV, Operating pressure, P_o = variable (Torr), Operating gas: Neon (Ne).

To start the numerical studies, the Lee code is configured with the above-mentioned parameters. Important details accompanying the dynamics of the plasma in the axial and radial phases are provided by the current derivative signal in Figure 2.1.

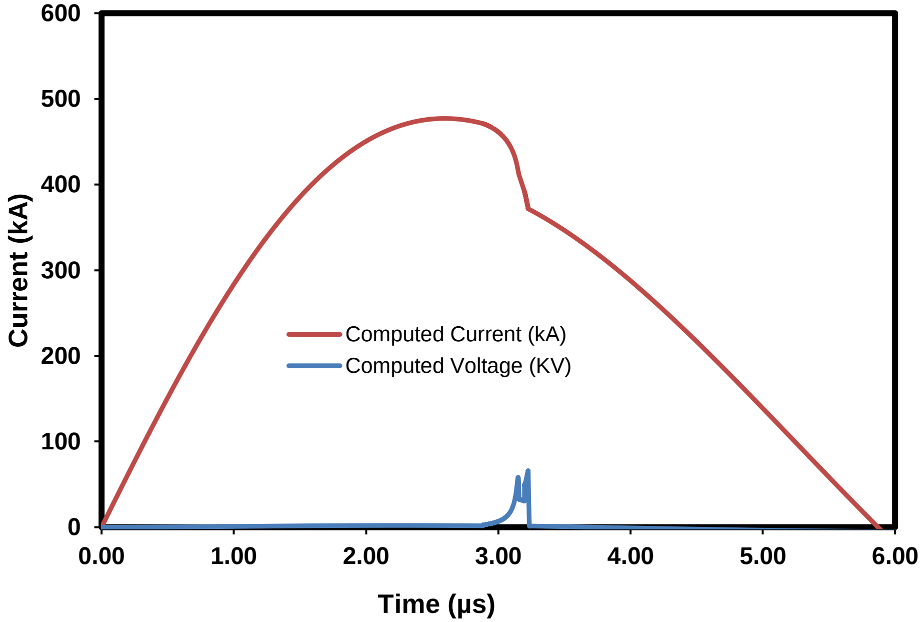

Figure 2.1: The computed current (red line) and voltage (blue line) trace in the BARC PF at 1.75 Torr Ne.

3. Results and Discussions

3.1 SXR yield with P_0 Variations

The dependence of the SXR yield of the BARC PF device on operating pressure has been studied using neon fill gas with a capacitor bank energy of 11.5 kJ (Table 3.1, Figure 3.1). The temperature of the pinch plasma, which is estimated to produce the SXR emission is between 2.3×10^6 and 5×10^6 K (200–500 eV). This is the temperature region in which neon is fully ionized and is, therefore, believed to be the most appropriate region for generating SXR.

It is found that the SXR yield increases monotonously with pressure, with its value being 17.7 J at 1 Torr, 69.4 J at 1.5 Torr, and 114.9 J at 1.75 Torr, respectively. The highest amount of energy, 137.9 J, was obtained at 2 Torr, but $T_{pinch} \simeq 2.07\times 10^6$ K is too low for the SXR emission window of neon. This is in spite of the fact that the absolute yield is greater than for experiments conducted at 2 Torr, indicating that the plasma conditions of 2 Torr are not as favorable for the production of line and continuum radiation. Hence, the effective maximum SXR yield of the device for neon is calculated to be 114.9 J at 1.75 Torr and well under the recommended operating temperature region. Therefore, the conversion efficiency is about 0.99% (≈1%) with respect to the total energy in the capacitor bank (11.5 kJ). This level of efficiency may be compared with that of earlier medium-energy plasma focus systems, which have previously known the SXR conversion efficiencies with neon in the range of 0.1%–1.5% (Abd Rashid *et al.*, 2015; Al-Hawat *et al.*, 2011; Hussain *et al.*, 2005; Neog *et al.*, 2006; Zhang *et al.*, 2005). Hence, these results reiterate that the BARC PF device can be compact, efficient source of pulsed SXR.

Table 3.1: Computed outcomes with P_0 variation of Ne in the 4.1 KJ PF.

P_0 (Torr)	I_{peak} (kA)	I_{pinch} (kA)	r_p (cm)	z_{max} (cm)	Pinch Duration (ns)	n_i pinch max $10^{23}/m^3$	T_{pinch} (× 10^6) k	Y_{sxr} (J/shot)
0.25	392	256	0.33	4.6	20.4	0.5	12.41	0.3
0.50	436	280	0.33	4.6	24.5	1.1	7.98	2.3
0.75	456	290	0.32	4.6	27.5	1.7	5.89	7.3
1.00	467	293	0.31	4.5	29.2	2.5	**4.59**	17.7
1.25	472	291	0.28	4.5	30.0	3.6	**3.69**	36.9
1.50	475	288	0.25	4.4	29.5	5.6	**3.02**	69.4
1.75	**477**	**282**	**0.21**	**4.4**	**28.0**	**9.6**	**2.48**	**114.9**
2.00	479	274	0.18	4.6	32.6	15.0	2.07	137.9
2.25	481	265	0.20	4.5	36.3	13.5	1.72	87.5
2.50	482	256	0.22	4.5	39.1	12.2	1.44	49.1
2.75	483	246	0.24	4.4	42.8	11.3	1.20	27.2
3.00	484	234	0.24	4.4	47.2	11.7	1.00	15.0

Such behavior can be understood through the equilibrium of plasma density and temperature during the compression. Even at the lower pressure (<1 Torr), although the pinch plasma temperature is higher than $T_{pinch} = 12 \times 10^6$ K at 0.25 Torr, plasma density is too low to generate much radiation. Starting from large pressures, the plasma density grows considerably, which enhances the bremsstrahlung and line emission. At the same time, the compression temperature is low enough to be favorable for neon radiation. The optimum condition for efficient SXR generation is obtained at a pressure of 1.75 Torr, where both the density and temperature are in their optimal ranges.

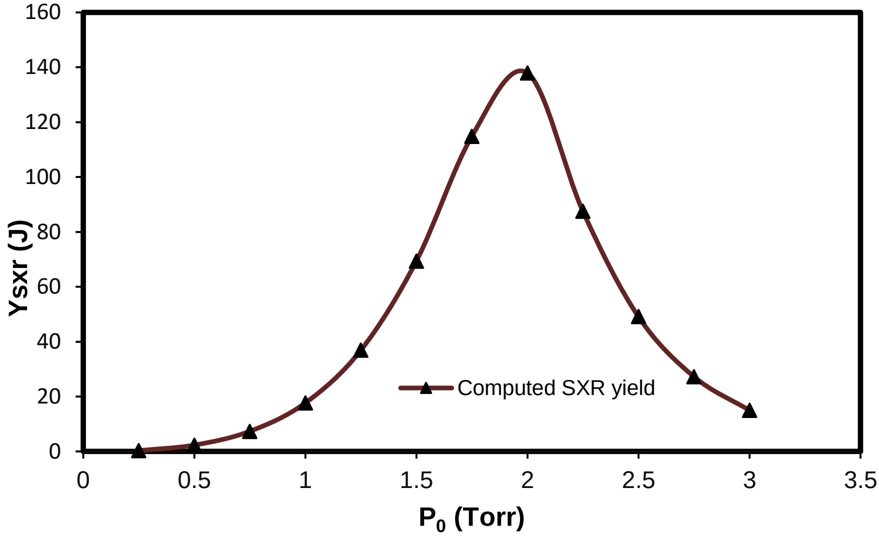

Figure 3.1: The change of computed Y_{sxr} vs P_0 with Ne gas in the BARC PF device.

Above 2 Torr, compression is saturated by the excessive mass loading, leading to lower plasma temperatures and emissivities, respectively. In general, the results confirm that the BARC PF is able to yield the desired neon SXR of 114.9 J/shot at 1.75Torr, which corresponds to about 1% of the input bank energy. Therefore, the device provides a reliable and efficient pulsed SXR source for material surface treatment, SXR lithography and plasma diagnostic applications. The computed discharge current waveforms of the BARC-PF device are illustrated in Figure 3.2 at various Ne filling pressures: 1.0, 1.25, 1.5, and 1.75 Torr. In all scenarios, the current escalates swiftly, reaching peak values of approximately ~460–480 kA around ~2.5 µs, followed by a sudden decline during the radial phase when the plasma pinch forms. The I_{peak} exhibits a modest rise with pressure, rising from 467 kA at 1 Torr to 477 kA at 1.75 Torr, which aligns reasonably with the values presented in Table 3.1.

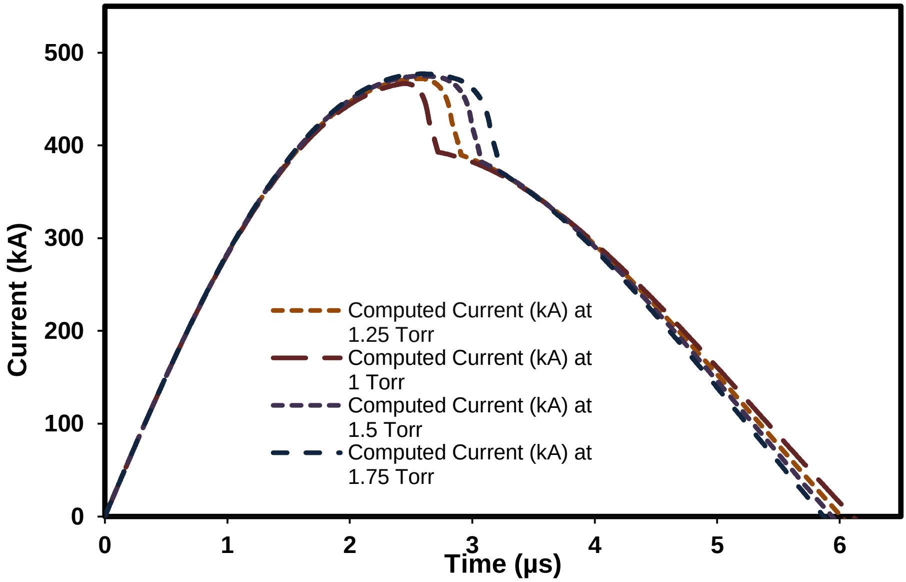

Figure 3.2: Computed current traces with P_0 variation with Ne gas in the BARC PF device.

However, the most important variance is the timing of the current depression. At reduced pressures (1 Torr), the current disruption occurs sooner, signifying a more expedited shock and diminished pinch formation duration. The current traces demonstrate a delay in the initiation of the dip as pressure escalates, signifying an extended run-down and pinch duration. This phenomenon arises from the augmented mass loading at elevated pressures, which interrupts the axial and radial phases, hence delaying the creation of the pinch, although it is sustained by increasing plasma densities. The minimal fluctuation in peak current relative to pressure variation across the whole range suggests that the total current supplied by the capacitor bank is only marginally affected by pressure changes. The pressure dependency primarily influences plasma dynamics and energy distribution during the pinch stage, which governs the efficiency of SXR and ion beam emission. The numerically computed current traces validate the numerical modeling of the BARC pulse-generating device and clearly illustrate the correlation between operating pressure, energy loading duration, and the performance of the PF. The diminished current at elevated pressures corresponds with an increase in the SXR yield, up to 1.75 Torr, indicating the synergistic optimization of electrical and plasma conditions for device functionality.

3.2 Optimization of Y_{sxr} with Electrode Configuration

In order to maximize the SXR yield of the BARC PF device, a parametric study was conducted using Neon as a fill gas and by changing anode and cathode radii (a and b) and P_0. The optimization was made under the constraint that the T_{pinch} was kept in the effective SXR emission window $2.3 \times 10^6 – 5 \times 10^6$ K. The results of changing

"a" for a fixed "$b = 6.1\ cm$" at 1.75 Torr are tabulated in Table 3.2. It clearly increases with "$\boldsymbol{a}$" up to 3.5 cm, to reach a maximum of 120.5 J/shot at a pinch temperature of 1.66 × 10^6 K. The current pinch increases for larger anode radii, while the plasma temperature is below the effective window, leading to very low yields.

Table 3.2: Computed Y_{sxr} with change of 'a' with 'b = 6.1 cm' at P_0 = 1.75 Torr in the BARC PF device.

a (cm)	**I_{peak} (kA)**	**I_{pinch} (kA)**	**r_p (cm)**	**z_{max} (cm)**	**Pinch Duration (ns)**	**n_i pinch max 10^{23}/m^3**	**T_{pinch} (× 10^6) k**	**Y_{sxr} (J/shot)**
2.5	467	290	0.23	3.7	24.3	5.4	3.74	34.8
3.0	**477**	**282**	**0.21**	**4.4**	**28.0**	**9.6**	**2.48**	**114.9**
3.5	485	268	0.22	5.4	44.4	11.0	1.66	120.5
4.0	492	250	0.33	6.0	63.8	6.9	1.10	49.2

The effect of the change of "b" is given in Table 3.3 with a constant "$a = 3\ cm$" at 1.75 Torr. The optimization results show that the SXR yield is maximized at $b = 6.8\ cm$ and the maximum value is 136.8 J/shot with a pinch temperature of 2.31 × 10^6 K just at the lower boundary of the neon SXR emitting range. A larger cathode radius continues to modestly increase the yield (to 139.7 J/shot at b = 7.0 cm), but now with the critical temperature dropping below 2.31 × 10^6 K, which takes us out of the operating regime range. Therefore, 136.8 J/shot is optimized yield with regard to the cathode geometry.

Table 3.3: Computed Y_{sxr} with change of 'b' with 'a = 3 cm' at P_0 = 1.75 Torr in the BARC PF device.

b (cm)	**I_{peak} (kA)**	**I_{pinch} (kA)**	**r_p (cm)**	**z_{max} (cm)**	**Pinch Duration (ns)**	**n_i pinch max 10^{23}/m^3**	**T_{pinch} (× 10^6) K**	**Y_{sxr} (J/shot)**
5.6	479	289	0.21	4.4	28.5	9.1	**2.61**	113.8
6.1	477	282	0.21	4.4	28.0	9.6	**2.48**	114.9
6.3	476	279	0.19	4.5	29.4	11.0	**2.44**	129.2
6.5	476	276	0.19	4.5	29.9	11.6	**2.39**	133.3
6.8	**475**	**272**	**0.18**	**4.5**	**30.6**	**12.4**	**2.31**	**136.8**
6.9	475	270	0.18	4.5	30.7	12.5	2.29	136.4
7.0	474	269	0.18	4.6	31.4	13.1	2.26	139.7

Finally, the effect of filling gas pressure (FGP) on the SXR emission for optimized electrode dimensions (a = 3 cm, b = 6.8 cm) is given in Table 3.4. The yield is rapidly increased with pressure, reaching 74 J/shot at 1.5 Torr, and maximizes at 136.8 J/shot at 1.75 Torr. Above this pressure, the yields decrease even with higher plasma densities, mostly because of an undershooting of the pinch

Table 3.4: Computed Y_{sxr} with P_0 variation at 'b = 6.8 cm' and 'a = 3 cm' in the BARC PF device.

P_0 (Torr)	I_{peak} (kA)	I_{pinch} (kA)	r_p (cm)	z_{max} (cm)	Pinch Duration (ns)	n_i pinch max $10^{23}/m^3$	T_{pinch} ($\times 10^6$) K	Y_{sxr} (J/shot)
0.25	396	257	0.34	4.6	20.4	0.5	12.50	0.3
0.50	438	280	0.33	4.6	24.6	1.1	7.96	2.3
0.75	457	288	0.32	4.6	27.6	1.7	5.80	7.4
1.00	465	288	0.31	4.5	29.5	2.5	**4.47**	18.2
1.25	469	285	0.28	4.5	30.0	3.7	**3.54**	38.3
1.50	472	280	0.24	4.4	29.3	6.0	**2.85**	73.9
1.75	**475**	**272**	**0.18**	**4.5**	**30.6**	**12.4**	**2.31**	**136.8**
2.00	477	262	0.18	4.6	34.6	13.9	1.88	112.1
2.25	479	251	0.21	4.5	38.2	11.9	1.54	61.4
2.50	480	239	0.23	4.4	42.0	10.8	1.26	31.6

temperature relative to the effective emission window. So, we can consider that the optimal trade-off between density and temperature is achieved for 1.75 Torr where the pinch temperature is at 2.31×10^6 K and the ∼1.2% yield of the total stored electronic capacitors energy (11.5 kJ).

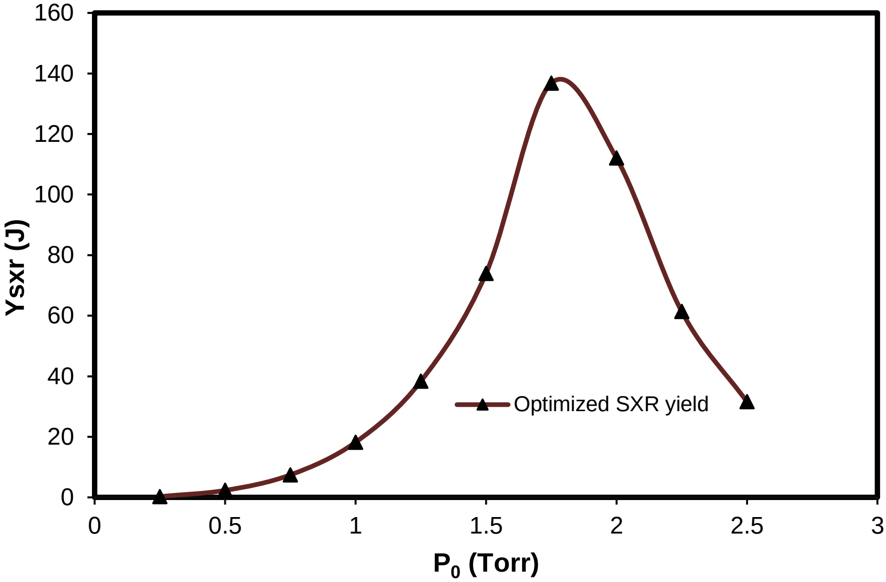

Figure 3.3: Optimized Y_{sxr} vs P_0 with Ne gas in the BARC PF device.

In conclusion, the parameter optimization shows that the highest maximum effective neon SXR yield of the BARC PF device is ~136–137 J/shot with a = 3 cm, b = 6.8 cm, and P_0 = 1.75 Torr (Figure. 3.3). Crucially, this yield is obtained at the given pinch plasma temperature window of $2.3 \times 10^6 - 5 \times 10^6$ K, indicating that geometric and pressure should be adjusted carefully to maximize the SXR output without detrimental effect on electron line radiation with neon.

3.3 Ion Beam Analysis

The ion beam properties of the BARC plasma PF device show a clear dependence on the FGP, the latter of which is presented in Table 3.5, Figures (3.4,3.5). The peak current (I_{peak}) rises with pressure from 436 kA at 0.5 Torr to the maximum value of 484 kA at 3 Torr, and the pinch current (I_{pinch}) exhibits a pressure dependence roughly similar to I_{peak} before 293 kA at 1 Torr, from where it decreases gradually to 234 kA at 3 Torr. The pinch radius (r_p) depends on pressure; it decreases with pressure and has a minimum (~0.18 cm) at 2 Torr and then slightly increases. The corresponding pinch duration (τ) also increases monotonically with pressure, from 24.5 ns at 0.5 Torr to 47 ns at 3 Torr, consistent with the longer confinement time at higher pressure.

Table 3.5: Ion Beam Properties Generated by the BARC PF Device for Various P_0.

Characteristics	**Pressure variation**									
P_0 (Torr)	**0.5**	**1**	**1.25**	**1.5**	**1.75**	**2**	**2.25**	**2.5**	**2.75**	**3**
I_{peak} (kA)	436	467	472	475	477	479	481	482	483	484
I_{peak}/a (kA/cm)	145	156	157	158	159	160	160	161	161	161
I_{pinch} (kA)	280	293	291	288	282	274	265	256	246	234
z_p (cm)	4.6	4.5	4.5	4.4	4.4	4.6	4.5	4.5	4.4	4.4
r_p (cm)	0.33	0.31	0.28	0.25	0.21	0.18	0.20	0.22	0.24	0.24
τ (ns)	24.5	29.2	30	29.5	28	32.6	36.3	39.1	42.8	47.2
V_{max} (kV)	72	63	60	59	66	57	55	52	48	44
Z_{eff}	10	9	8	8	8	8	8	8	8	8
Ion fluence ($\times 10^{19}$ m^{-2})	3.06	5.27	6.69	8.91	12.9	20.5	16.9	13.7	11.8	10.3
Ion flux ($\times 10^{27}$ m^{-2}s^{-1})	1.25	1.80	2.23	3.02	4.62	6.30	4.67	3.50	2.76	2.17
Ion energy ($\times 10^{3}$ keV)	2.15	1.65	1.53	1.45	1.40	1.37	1.31	1.24	1.16	1.04
En fluence ($\times 10^{7}$ J m^{-2})	1.05	1.39	1.64	2.07	2.90	4.5	3.56	2.73	2.19	1.72
En flux ($\times 10^{14}$ Wm^{-2})	4.3	4.8	5.5	7	10.4	13.8	9.8	7	5.1	3.6
Ion number/kJ ($\times 10^{14}$)	0.9	1.37	1.48	1.52	1.50	1.74	1.80	1.79	1.83	1.88
FIB energy (J)	356	415	417	408	387	440	435	412	390	362
FIB current (kA)	67.1	75.4	76.7	77.7	78.9	78.9	73	67	63	58.6
Beam power ($\times 10^{10}$ W)	1.46	1.42	1.39	1.38	1.38	1.35	1.20	1.05	0.91	0.77
Dam Fr ($\times 10^{10}$ Wm^{-2}s$^{0.5}$)	6.7	8.1	9.5	12.1	17.3	24.9	18.7	13.8	10.6	7.9
Ion speed (cm/μs)	144	134	131	130	129	127	125	121	117	112
FPS En (J)	745	831	850	862	882	803	766	738	704	672
FPS En (% E_0)	6.5	7.2	7.4	7.5	7.7	7	6.6	6.4	6.1	5.8
FPS speed (cm/μs)	48	38	36	37	40	42	34	28	24	20

The ion fluence shows non-monotonic dependence, and it rises abruptly from 3.06 × 10^{19} m^{-2} at 0.5 Torr to the maximum of 2.05 × 10^{20} m^{-2} at 2 Torr, then declines with increasing pressure. Ion flux also exhibits the same pattern, with a maximum of 6.30 × 10^{27} m^{-2}s^{-1} at 2 Torr. At 0.5 Torr, the ion energy per particle is about 2.15

keV, but at 3 Torr, it's only 1.04 keV. This means that higher pressure makes each ion less energetic and increases the output of ions.

Additionally, this compromise is demonstrated by the sum of all focused ion beam (FIB) energy, which reaches a maximum of approximately 440 J at 2 Torr and then continues to decrease. The effective ion beam power is similarly pressure-sensitive; it stays nearly constant (~1.3 – 1.4 × 10^{10} W) between 0.5 and 1.75 Torr and begins to drop at higher gas pressure levels. According to the mean ion energy scaling, the ions' speed decreases gradually with pressure, from around 144 cm/μs at 0.5 Torr to about 112 cm/μs at 3 Torr.

.

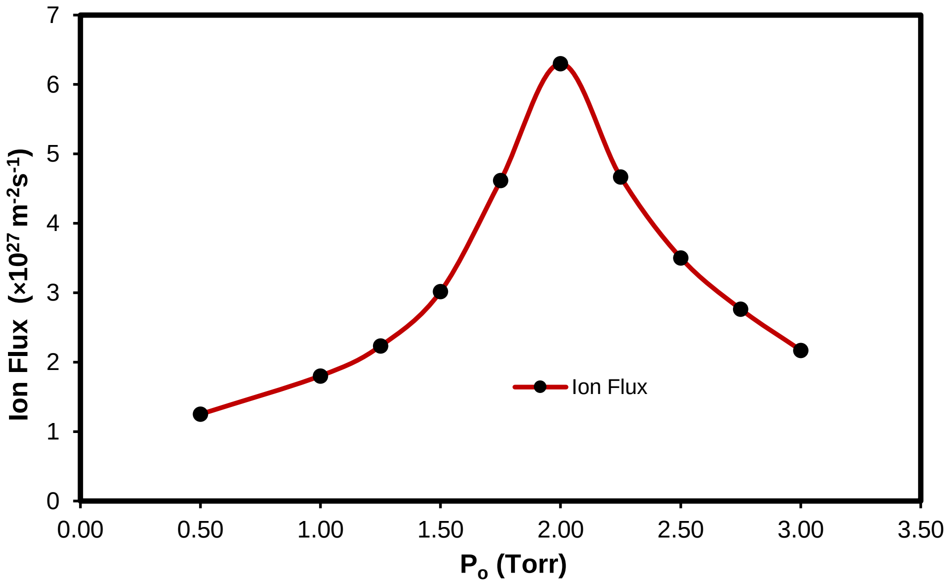

Figure 3.4: The change of computed Ion flux vs P_o with Ne gas in the BARC PF device.

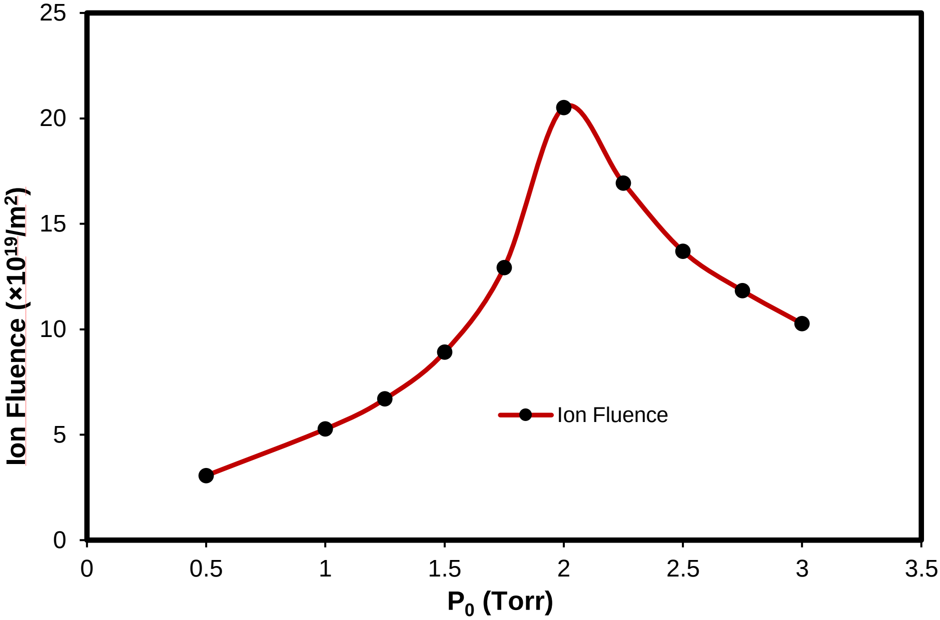

Figure 3.5: The change of computed Ion fluence vs P_o with Ne gas in the BARC PF device.

In conclusion, the focus is on an ideal pressure window of roughly 1.75–2.0 Torr that provides sufficient confinement and pinch stability along with a favorable trade-off between ion fluence, flux, and beam energy. At lower pressures, the system produces high-energy ions but less ion fluence. However, at higher pressures, the ion fluence is significantly lower, even though the confinement time is longer. These patterns highlight the necessity of controlling pressure when designing PF-driven ion beams for uses such as surface modification, material processing, and nuclear fusion studies.

4. Radial Trajectories of BARC PF

The impact of FGP on the radial phase dynamics of the PF device was analyzed at pressures of 1.0, 1.25, 1.5, and 1.75 Torr, as illustrated in Figure 3.6 [(a)–(d)]. The results indicate a clear monotonic dependence of the shock, piston, and pinch evolution on the operating pressure. At 1.0 Torr [Figure 3.6(a)], the radial inward shock propagates with the highest velocity, reaching the axis within ~250 ns, while the associated piston stagnates relatively early, resulting in limited pinch elongation and the earliest occurrence of the reflected shock. Increasing the pressure to 1.25 Torr [Figure 3.6(b)] reduces the shock velocity, introduces a larger piston–shock separation, and extends the pinch column length. At the larger pressures of 1.5 and 1.75 Torr [Figure 3.6(c, d)], the radial implosion is significantly slowed down with

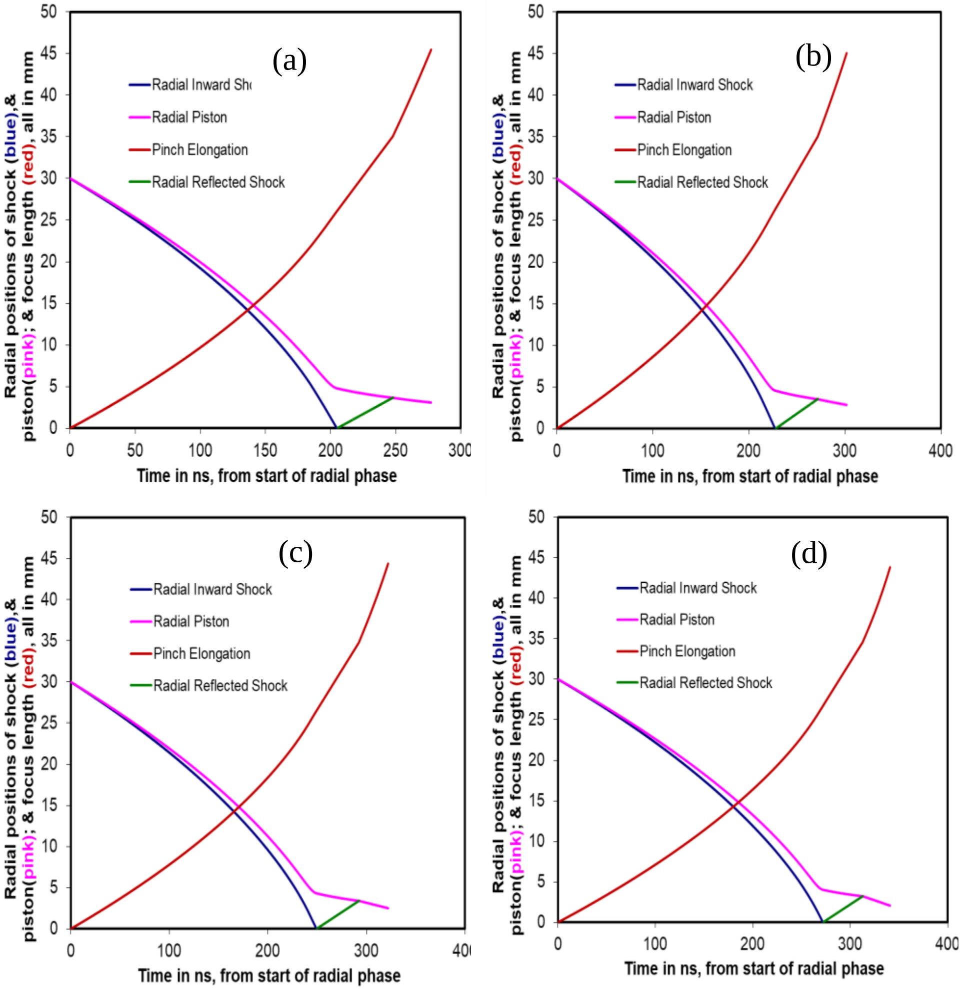

Figure 3.6: Radial trajectories with Ne gas at (a) 1 Torr, (b) 1.25 Torr, (c) 1.5 Torr, and (d) 1.75 Torr in the BARC PF device.

the convergence times of ~300 ns. The piston is delayed considerably from the shock front, and the reflected shock is seen at successively later times. In parallel, the pinch elongation grows with pressure, with a peak at 1.75 Torr. This is explained by an increased mass loading at higher pressure, which decreases the implosion velocity and extends the radial phase, thereby supporting a longer plasma column. These facts indicate that the higher the FGP, the more the PF radial phase changes in a systematic way toward shock converging and formation of reflected shock, and the pinch is more elongated. These trends are consistent with those predicted on theoretical grounds of mass-dependent implosion dynamics and are relevant in the optimized operation of PF for pressure-variable systems.

5. Conclusion

The pressure and geometry-dependent behaviours of both SXR emission and the ion beam generation with neon filling gas have been numerically studied for the BARC PF device with the Lee model code. The results of the study confirm that the effective neon SXR pinch plasma temperature window ranges between the values of 2.3×10^6 and 5×10^6 K, and at 1.75 Torr, the highest effective yield of 114.9 J (which corresponds to 1% of the capacitor bank energy) was obtained. An additional optimization of the electrode dimensions increased the SXR yield to 137 J/shot with a = 3cm, b = 6.8cm, P_0 = 1.75 Torr and a conversion efficiency of ~1.2%. The ion beam results demonstrate that the ion fluence and flux increased with pressure up to 2 Torr, and when the focused ion beam energy was ~440 J at this condition, the performance began to degenerate due to the lower ion energy. This defines an optimal pressure window of around 1.75–2 Torr for both improved SXR and ion beam outputs. Generally, the results demonstrate the ability of the BARC PF device to be a compact, efficient source of pulsed SXR radiation and energetic ion beams. These results offer useful assistance for experimental optimization and applications for plasma diagnostics, material science, and inertial confinement fusion research.

Acknowledgement

The author acknowledges his heartfelt appreciation to Dr Sing Lee for granting access to the Lee Code and the Physics Department, IUBAT, for providing the sound environment.

References

Abd Rashid, N., Mohamad, S. N., Chaudhary, K. T., Lee, S., Saw, S. H., & Ali, J. (2015). Effects of approximation and close-fitting technique of corona model on neon soft X-ray emission in 3-kJ plasma focus. *IEEE Transactions on Plasma Science, 43*(7), 2146–2154.

Akel, M., Salo, S. A., Saw, S. H., & Lee, S. (2014). Ion Beam Features Produced by Two Plasma Focus Machines Operated With Different Gases. *IEEE Transactions on Plasma Science, 42*(9), 2202–2206. https://doi.org/10.1109/TPS.2014.2342743

Akel, M., Lee, S., & Saw, S. H. (2012). Numerical Experiments in Plasma Focus Operated in Various Gases. *IEEE Transactions on Plasma Science, 40*(12), 3290–3297. https://doi.org/10.1109/TPS.2012.2220863

Akel, M., Salo, S. A., Saw, S. H., & Lee, S. (2014). Properties of Ion Beams Generated by Nitrogen Plasma Focus. *Journal of Fusion Energy, 33*(2), 189–197. https://doi.org/10.1007/s10894-013-9660-7

Al-Hawat, Sh., Akel, M., & Lee, S. (2011). Numerical Experiments on Neon Soft X-Ray Optimization of AECS-PF2 Plasma Focus Device. *Journal of Fusion Energy, 30*(6), 494–502. https://doi.org/10.1007/s10894-011-9416-1

Ali, J. (1990). Development and studies of a small plasma focus. Ph. D. Dissertation.

Beg, F., Ross, I., Lorenz, A., Worley, J., Dangor, A., & Haines, M. (2000). Study of x-ray emission from a table top plasma focus and its application as an x-ray backlighter. *Journal of Applied Physics, 88*(6), 3225–3230.

Boggasch, E., Jacoby, J., Wahl, H., Dietrich, K.-G., Hoffmann, D. H. H., Laux, W., Elfers, M., Haas, C. R., Dubenkov, V. P., & Golubev, A. A. (1991). Z -pinch plasma lens focusing of a heavy-ion beam. *Physical Review Letters, 66*(13), 1705–1708. https://doi.org/10.1103/PhysRevLett.66.1705

Castillo-Mejía, F., Milanese, M. M., Moroso, R. L., Pouzo, J. O., & Santiago, M. A. (2001). Small plasma focus studied as a source of hard X-ray. *IEEE Transactions on Plasma Science, 29*(6), 921–926.

Fortov, V., Dyabilin, K., Lebedev, M., Grabovskij, E., Smirnov, V., Sharkov, B., Golubev, A., Hoffmann, D. H. H., & Eidmann, K. (1998). The application of high intensive Z-pinch radiation and heavy ion beams for research on high energy density physics. In *12th International Conference on High-Power Particle Beams. BEAMS'98. Proceedings (Cat. No.98EX103), 1*, 89–94. https://doi.org/10.1109/BEAMS.1998.822395

Gribkov, V. A., Srivastava, A., Keat, P. L. C., Kudryashov, V., & Lee, S. (2002). Operation of NX2 dense plasma focus device with argon filling as a possible radiation source for micro-machining. *IEEE Transactions on Plasma Science, 30*(3), 1331–1338.

Hayashi, T., Matsumuro, A., Muramatsu, M., Kohzaki, M., Takahashi, Y., & Yamaguchi, K. (1999). Structural analysis of a carbon nitride film prepared by ion-beam-assisted deposition. *Japanese Journal of Applied Physics, 38*(4A), L395.

Hussain, S., Shafiq, M., Ahmad, R., Waheed, A., & Zakaullah, M. (2005). Plasma focus as a possible x-ray source for radiography. *Plasma Sources Science and Technology, 14*(1), 61.

Kato, Y., Ochiai, I., Watanabe, Y., & Murayama, S. (1988). Plasma focus x-ray source for lithography. *Journal of Vacuum Science & Technology B: Microelectronics Processing and Phenomena, 6*(1), 195–198. https://doi.org/10.1116/1.584044

Lee, S. (1991). A sequential plasma focus. *IEEE Transactions on Plasma Science, 19*(5), 912–919.

Lee, S., Lee, P., Zhang, G., Feng, X., Gribkov, V. A., Liu, M., Serban, A., & Wong, T. K. (1998). High rep rate high performance plasma focus as a powerful radiation source. *IEEE Transactions on Plasma Science, 26*(4), 1119–1126.

Lee, S., & Saw, S. H. (2012). Plasma focus ion beam fluence and flux—Scaling with stored energy. *Physics of Plasmas, 19*(11), 112703. https://pubs.aip.org/aip/pop/article/19/11/112703/124628

Lee, S., & Saw, S. H. (2013). Plasma focus ion beam fluence and flux—For various gases. *Physics of Plasmas, 20*(6), 062702. https://doi.org/10.1063/1.4811650

Lee, S., & Serban, A. (1996). Dimensions and lifetime of the plasma focus pinch. *IEEE Transactions on Plasma Science, 24*(3), 1101–1105.

Lee, S., Tou, T., Moo, S., Eissa, M., Gholap, A., Kwek, K., Mulyodrono, S., Smith, A., Suryadi, & Usada, W. (1988). A simple facility for the teaching of plasma dynamics and plasma nuclear fusion. *American Journal of Physics, 56*(1), 62–68.

Mather, J. W. (1965). Formation of a High-Density Deuterium Plasma Focus. *The Physics of Fluids, 8*(2), 366–377. https://doi.org/10.1063/1.1761231

Mather, J. W. (1971). 15. Dense Plasma Focus. In R. H. Lovberg & H. R. Griem (Eds.), *Methods in Experimental Physics* (Vol. 9, pp. 187–249). Academic Press. https://doi.org/10.1016/S0076-695X(08)60862-5

McNamara, B. (1984). Radiation in Plasmas, Volume II.

Neog, N. K., Mohanty, S. R., & Hotta, E. (2006). Anode length optimization in a modified plasma focus device for optimal x-ray yields. *Journal of Applied Physics, 99*(1). https://pubs.aip.org/aip/jap/article/99/1/013302/923100

Pavez, C., & Soto, L. (2010). Demonstration of X-ray emission from an ultraminiature pinch plasma focus discharge operating at 0.1 J nanofocus. *IEEE Transactions on Plasma Science, 38*(5), 1132–1135.

Pereira, N. R., & Davis, J. (1988). X rays from Z -pinches on relativistic electron-beam generators. *Journal of Applied Physics, 64*(3), R1–R27. https://doi.org/10.1063/1.341808

Petr, R., Bykanov, A., Freshman, J., Reilly, D., Mangano, J., Roche, M., Dickenson, J., Burte, M., & Heaton, J. (2004). Performance summary on a high power dense plasma focus x-ray lithography point source producing 70 nm line features in AlGaAs microcircuits. *Review of Scientific Instruments, 75*(8), 2551–2559.

Plasma Focus (Radiative) Computation Model. Retrieved February 8, 2024, from http://www.intimal.edu.my/school/fas/UFLF/File1RADPF.htm

Rawat, R., Zhang, T., Lim, G., Tan, W., Ng, S., Patran, A., Hassan, S., Springham, S., Tan, T., & Zakaullah, M. (2004). Soft X-ray imaging using a neon filled plasma focus X-ray source. *Journal of Fusion Energy, 23*(1), 49–53.

Rosiński, M., Badziak, J., Boody, F. P., Gammino, S., Hora, H., Krása, J., Láska, L., Mezzasalma, A. M., Parys, P., & Rohlena, K. (2005). Application of laser ion source for ion implantation technology. *Vacuum, 78*(2–4), 435–438.

Sadowski, M., Langner, J., Stanisławski, J., Matejicek, J., Kolman, B., & Chráska, P. (2000). Surface modification of plasma-sprayed alumina deposits by high-energy ion beams. *Nukleonika, 45*(3), 199–202.

Saw, S. H. (1990). *Experimental Studies of a Current-stepped Z-pinch* (Doctoral dissertation, Jabatan Fizik, Fakulti Sains, Universiti Malaya).

Shi, W., Wu, J. D., Sun, J., Ling, H., Ying, Z. F., Ding, X. M., Zhou, Z. Y., & Li, F. M. (2001). Formation of CNx thin films by reactive pulsed laser deposition assisted by electron cyclotron resonance microwave discharge. *Applied Physics A*, *73*(5), 605–608.

Singh, A., Heoh, S. S., & Sing, L. (2017). Numerical study on the variation of pressure on India Bhabha Atomic Research Center (BARC) and Imperial College plasma focus machines. *AIP Conference Proceedings*, *1824*(1), 030002. https://doi.org/10.1063/1.4978820

Saw S. H., Lee, S., P. C. K., Rawat, R. S., & Sing Lee. (2009). Optimizing UNU/ICTP PFF Plasma Focus for Neon Soft X-ray Operation. *IEEE Transactions on Plasma Science, 37*(7), 1276–1282. https://doi.org/10.1109/TPS.2009.2022167

Soto, L., Silva, P., Moreno, J., Zambra, M., Kies, W., Mayer, R. E., Clausse, A., Altamirano, L., Pavez, C., & Huerta, L. (2008). Demonstration of neutron production in a table-top pinch plasma focus device operating at only tens of joules. *Journal of Physics D: Applied Physics, 41*(20), 205215.

The Universal Plasma Focus Machine. (n.d.). Retrieved February 8, 2024, from https://www.plasmafocus.net/IPFS/modelpackage/UPF.htm

Tomida, M., Kato, Y., & Asaji, T. (2005). Formation of β-FeSi2 by implanting multicharged iron ions produced in an ECR ion source. *Nuclear Instruments and Methods in Physics Research Section B: Beam Interactions with Materials and Atoms, 237*(1–2), 83–87.

Tong, Z. S., Wu, M. Z., Pu, T. S., Zhou, F., & Liu, H. Z. (1995). Ion-beam-induced electrical conductivity in plasma-polymerized aniline film. *Synthetic Metals*, *68*(2), 125–131.

Tou, T., Lee, S., & Kwek, K. (1989). Nonperturbing plasma-focus measurements in the run-down phase. *IEEE Transactions on Plasma Science*, *17*(2), 311–315.

Velikovich, A. L., Clark, R. W., Davis, J., Chong, Y. K., Deeney, C., Coverdale, C. A., Ruiz, C. L., Cooper, G. W., Nelson, A. J., Franklin, J., & Rudakov, L. I. (2007). Z-pinch plasma neutron sources. *Physics of Plasmas*, *14*(2), 022701. https://doi.org/10.1063/1.2435322

Verma, R., Roshan, M. V., Malik, F., Lee, P., Lee, S., Springham, S. V., Tan, T. L., Krishnan, M., & Rawat, R. S. (2008). Compact sub-kilojoule range fast miniature plasma focus as portable neutron source. *Plasma Sources Science and Technology, 17*(4), 045020. https://doi.org/10.1088/0963-0252/17/4/045020

Wahbe, S., Abou-Ali, Y., Akel, M., Lee, S., & Marciniak, L. (2023). Numerical experiments on the total D–D fusion neutron yield versus deuterium pressure for different energy plasma focus devices using the Lee model code. *Plasma Physics and Controlled Fusion*, *65*(5), 055022. https://doi.org/10.1088/1361-6587/acc610

Wen, L. S., Jiang, X., & Si, C. Y. (1986). A transmission electron microscopy study on Ti–N films deposited by ion plating. *Journal of Vacuum Science & Technology A: Vacuum, Surfaces, and Films*, *4*(6), 2682–2685.

Wong, D., Patran, A., Tan, T., Rawat, R., & Lee, P. (2004). Soft X-ray optimization studies on a dense plasma focus device operated in neon and argon in repetitive mode. *IEEE Transactions on Plasma Science*, *32*(6), 2227–2235.

Yatsui, K., Grigoriu, C., Masugata, K., Jiang, W. J. W., & Sonegawa, T. S. T. (1997). Preparation of thin films and nanosize powders by intense, pulsed ion beam evaporation. *Japanese Journal of Applied Physics, 36*(7S), 4928.

Zhang, T., Lin, X., Chandra, K. A., Tan, T. L., Springham, S. V., Patran, A., Lee, P., Lee, S., & Rawat, R. S. (2005). Current sheath curvature correlation with the neon soft x-ray emission from plasma focus device. *Plasma Sources Science and Technology*, *14*(2), 368.